Eur J Cancer Clin Oncol, Vol. 24, No. 7, pp. 1139–1150, 1988.
Printed in Great Britain

0277-5379/88$3.00+0.00

Uncoupling of Hexose Transport and Phosphorylation in Human Gliomas Demonstrated by PET

KARL HERHOLZ, PETER ZIFFLING, WOLFGANG STAFFEN, GUNTER PAWLIK, RAINER WAGNER, KLAUS WIENHARD and WOLF-DIETER HEISS

Max-Planck-Institut für neurologische Forschung und Universitätsnervenklinik—Schwerpunkt Neurologie, Joseph-Stelzmann-Str. 9, 5000 Köln 41 (Lindenthal), F.R.G.

Abstract—*Tumor uptake of [^{18}F]2-fluoro-2-deoxy-glucose (FDG) was studied in 20 patients with histologically classified gliomas, using dynamic positron emission tomography (PET).*

Parametric images of local blood volume, glucose metabolic rate, transport and phosphorylation rate constants were generated by weighted non-linear least-squares fits on a pixel-by-pixel basis. Tumor metabolism, i.e. ratios of tumor peak metabolism to contralateral brain metabolism, corresponded with histological grade. Approximately half of the tumors showed considerable metabolic heterogeneity, and metabolically active areas were found in the periphery of seven tumors. Rate constants of FDG transport and phosphorylation were significantly correlated and were inversely coupled to plasma glucose levels in contralateral brain. In contrast, tumor transport and phosphorylation rate constants varied independently of each other and of plasma glucose concentration. In some tumors large alterations of FDG phosphorylation were observed in presence of nearly normal FDG transport.

INTRODUCTION

BIOCHEMICAL *in vitro* experiments have shown that glucose transport and phosphorylation may be altered in gliomas and other brain tumors [1–3]. Therefore, positron emission tomography (PET) after application of the glucose analog [^{18}F]2-fluoro-2-deoxyglucose (FDG) has been used for *in vivo* diagnosis of tumors, and a correlation between histological grading and FDG uptake has been demonstrated [4, 5].

In the present study, two refinements of the PET–FDG technique were used in order to elucidate the relation between FDG transport and phosphorylation in human brain tumors *in vivo*, rather than examining only total FDG uptake. First, the time course of FDG accumulation was recorded by dynamic PET scanning, and second, the time activity curves were analyzed on a pixel-by-pixel basis, yielding parametric images of local blood volume, FDG transport and phosphorylation, and glucose metabolic rate, in order to account as far as possible for tumor heterogeneity. With this technique, some tumors could be identified in which regional alterations of FDG uptake were almost exclusively caused by changes of hexokinase activity. Generally, tumors showed large variability of FDG transport and phosphorylation rate constants. They were uncoupled from their normal dependence on competing plasma glucose levels.

Accepted 22 December 1987.
Address for correspondence and reprint requests: Prof. Dr. W.-D. Heiss, Universitätsnervenklinik—Schwerpunkt Neurologie, Joseph-Stelzmann-Str. 9, D-5000 Köln 41 (Lindenthal), F.R.G.

PATIENTS AND METHODS

Included were the PET studies of 20 consecutive patients with histologically proven gliomas. Ages ranged between 10 and 74 years (mean 45.7), nine were females, 11 males. All patients had X-ray CT scans with and without intravenous application of contrast material.

Eleven patients were studied before any specific tumor therapy other than corticosteroids was initiated. Eight patients had been operated on, in one case by stereotaxic biopsy only, six had received radiation therapy, four chemotherapy (CCNU), before their PET examination.

Histological classification according to current WHO criteria was based on specimens obtained during open tumor resection in 15 cases, by open biopsy in one, by stereotaxic biopsy in two, and by autopsy in another two cases. Four tumors were of grade II, three of grade III, eight of grade IV,

Table 1. *Patient data*

Patient No.	Age (years)	Sex	Side	Tumor location	Specimen	Tumor grade	Therapy before PET		
							Oper.	Rad.	Chemoth.
1	49	F	L	Parietal	Biopsy	2	N	N	N
2	29	F	L	Frontal	Resection	2	N	N	N
3	41	F	R	Frontal	Resection	2	N	N	N
4	46	M	R	Midbrain	Biopsy	2	N	N	N
5	48	F	R	Temporal	Resection	3	N	N	N
6	52	M	R	Parietal	Resection	3	N	N	N
7	57	M	R	Temporal	Biopsy	3	N	N	N
8	74	F	L	Temporal	Resection	4	N	N	N
9	46	M	L	Parietal	Resection	4	Y	Y	Y
10	64	M	R	Parietal	Resection	4	N	N	N
11	66	M	R	Temporal	Resection	4	N	N	N
12	53	M	R	Temporal	Autopsy	4	N	Y	Y
13	49	F	L	Frontal	Resection	4	Y	Y	Y
14	10	M	R	Thalamus	Autopsy	4	Y	N	N
15	45	M	R	Parietal	Resection	4	N	N	N
16	59	F	L	Temporal	Resection	2 (R)	Y	Y	N
17	39	M	L	Frontal	Resection	3 (R)	Y	Y	Y
18	27	F	R	Frontal	Resection	2 (R)	Y	N	N
19	34	M	R	Temporal	Resection	3 (R)	Y	Y	N
20	25	F	L	Frontal	Resection	2 (R)	Y	N	N

Recurrent tumors are marked by (R) in column 'Tumor grade'.

and five were recurrencies of tumors previously classified as grade II or III. All tumors were astrocytomas or glioblastomas, respectively. Five tumors were located in the parietal, seven in the temporal, six in the frontal lobe, and two in deep brain structures (brainstem and thalamus). All pertinent patient data are listed in Table 1.

PET measurements

Patients were examined in a resting state with eyes closed and ears unplugged. Each received a rapid intravenous bolus injection of approx. 5 mCi (185 MBq) FDG, synthesized according to Ido *et al.* [6] or Ehrenkaufer *et al.* [7]. Sequential scanning (scan intervals 5× 1 min, 5 × 2 min, 5 × 3 min, 2 × 5 min) was started at the time of injection, with a total measurement of 40 min. Total scanner count rates were continuously monitored by a rate meter in order to determine the time of bolus arrival in the brain. Starting at the time of bolus arrival in the brain, approx. 20–22 blood samples were drawn from a dorsal hand vein heated to 44°C in a water bath, with initial sampling as fast as possible and at progressively larger intervals after 2 min. Data of seven slices parallel to the canthomeatal plane, each approx. 11 mm thick, were simultaneously acquired using a Scanditronix PC 384 PET scanner [8], and images were reconstructed by filtered backprojection with appropriate corrections for attenuation and scatter [9, 10].

An active spatial filter was applied to the reconstructed series of tomograms. This filter was especially designed to improve the signal-to-noise ratio in sequential tomograms, using simple statistical criteria; simulation studies ensured that it did not disturb image quantitation. For each pixel, the rate constants for FDG transport (K_1 from blood to tissue, k_2 reverse) and phosphorylation (k_3) were calculated. Metabolic rates (MR) were computed from these individual rate constants using the model described previously by Heiss *et al.* [11] with a lumped constant of 0.42. Calculations were done by nonlinear least-squares fitting, using the number of total counts per slice as an estimate of the variance of data points for weighting. A local blood volume term was included in the fitting procedure, as suggested by Hawkins *et al.* [12] and Evans *et al.* [13]. In order to accelerate the fits and to avoid the problem of false local minima, starting values were generated by a combination of the methods of Patlak *et al.* [14] and Alpert *et al.* [15]. Parametric images of blood volume, transport (K_1) and phosphorylation (k_3) rate constants, as well as of the glucose metabolic rate were used for data analysis.

Circular regions including the whole tumor bulk as judged on the basis of corresponding X-ray CT scans were superimposed onto the parametric images and mean parameter values were calculated within each region. If the tumor extended across several slices, averages weighted by region size were calculated. In addition, the tumor peak metabolic rate was determined. For comparison average par-

Table 2. PET results

Patient No.	Plasma glucose	Tumor Peak MR	Tumor Mean MR	Tumor Mean K_1	Tumor Mean k_3	Tumor Mean blood volume	Contralateral brain (mean values) MR	Contralateral brain (mean values) K_1	Contralateral brain (mean values) k_3	Contralateral brain (mean values) Blood volume
1	4.44	35	14.0	0.056	0.018	0.038	28.2	0.083	0.055	0.032
2	7.10	23	9.1	0.034	0.016	0.013	22.0	0.067	0.035	0.044
3	5.21	30	16.2	0.073	0.026	0.050	22.7	0.081	0.045	0.068
4	5.77	21	8.1	0.030	0.025	0.041	25.3	0.102	0.033	0.062
5	6.60	54	35.5	0.065	0.053	0.028	16.3	0.054	0.024	0.022
6	5.93	31	22.1	0.086	0.028	0.075	22.1	0.071	0.051	0.052
7	5.99	15	10.0	0.090	0.011	0.046	17.7	0.070	0.031	0.034
8	4.55	40	14.0	0.038	0.038	0.025	24.2	0.068	0.060	0.030
9	19.75	51	20.7	0.034	0.015	0.031	16.9	0.028	0.013	0.030
10	10.60	29	18.7	0.055	0.022	0.058	23.4	0.064	0.025	0.062
11	7.52	36	11.4	0.035	0.019	0.142	24.0	0.064	0.046	0.165
12	6.10	31	21.2	0.068	0.046	0.056	21.4	0.071	0.041	0.056
13	5.99	25	19.2	0.065	0.038	0.025	19.2	0.077	0.034	0.039
14	5.21	40	12.7	0.104	0.017	0.072	23.8	0.083	0.042	0.059
15	6.04	79	32.8	0.069	0.050	0.053	19.1	0.069	0.032	0.034
16	5.43	75	24.3	0.093	0.042	0.043	20.5	0.068	0.045	0.035
17	5.99	33	9.0	0.023	0.019	0.007	27.1	0.072	0.047	0.021
18	7.24	42	26.6	0.043	0.047	0.060	23.6	0.048	0.041	0.070
19	4.66	34	12.1	0.046	0.025	0.014	23.5	0.076	0.054	0.028
20	4.17	33	14.4	0.049	0.028	0.039	29.9	0.082	0.057	0.067
Mean ± S.D.	6.72 ±3.377	37.9 ±16.27	17.6 ±7.78	0.058 ±0.0231	0.030 ±0.0131	0.046 ±0.0294	22.6 ±3.59	0.070 ±0.0151	0.041 ±0.0122	0.051 ±0.0314

Units: plasma glucose, mmol/l; MR, μmol/100 g/min; K_1, ml/g/min; k_3, 1/min; blood volume, ml/g.

ameters were also determined in the whole contralateral hemisphere at the level of the centrum semiovale.

RESULTS

Comparing the parameters of all tumors with the corresponding values of contralateral brain (Table 2), mean FDG transport and metabolism was significantly lower ($P < 0.05$, paired t-test) in tumors. A wide range of metabolic rates was observed in tumors, with peak values from 15 to 79 μmol/100 g/min and mean values from 8.1 to 35.5 μmol/100 g/min.

No significant effect of patient age and gender on tumor parameters was found. The four metabolically most active tumors were located in the parietal and temporal lobes, but no significant effect of tumor location on metabolism could be demonstrated.

There was a trend of high-grade tumors towards higher peak metabolic rates (Fig. 1a). Excluding recurrent tumors, a significant rank correlation with histological grade was obtained for the ratios of peak MR over contralateral brain MR (Kendall's tau $B = 0.449$, $P = 0.036$; Fig. 1b).

The correlation of mean tumor MR and individ-

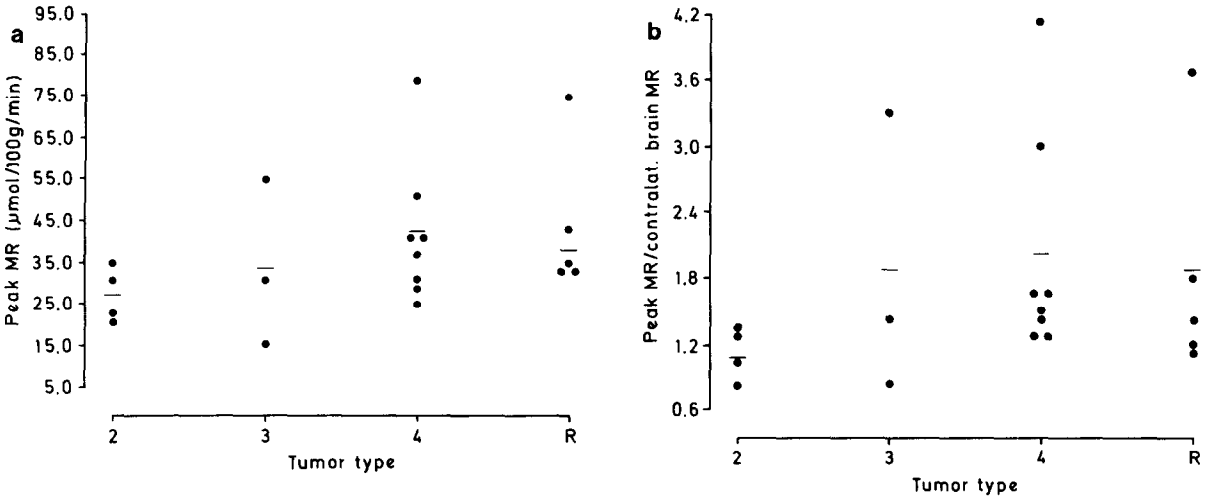

Fig. 1. Tumor peak metabolic rates (a: absolute values, b: ratio with reference to contralateral brain) in histological classes (2, 3, 4 indicate tumor grade, R represents recurrent tumors of previous grade 2 or 3). A trend towards higher metabolic rates in malignant tumors is obvious, with relatively high rates also in recurrent tumors.

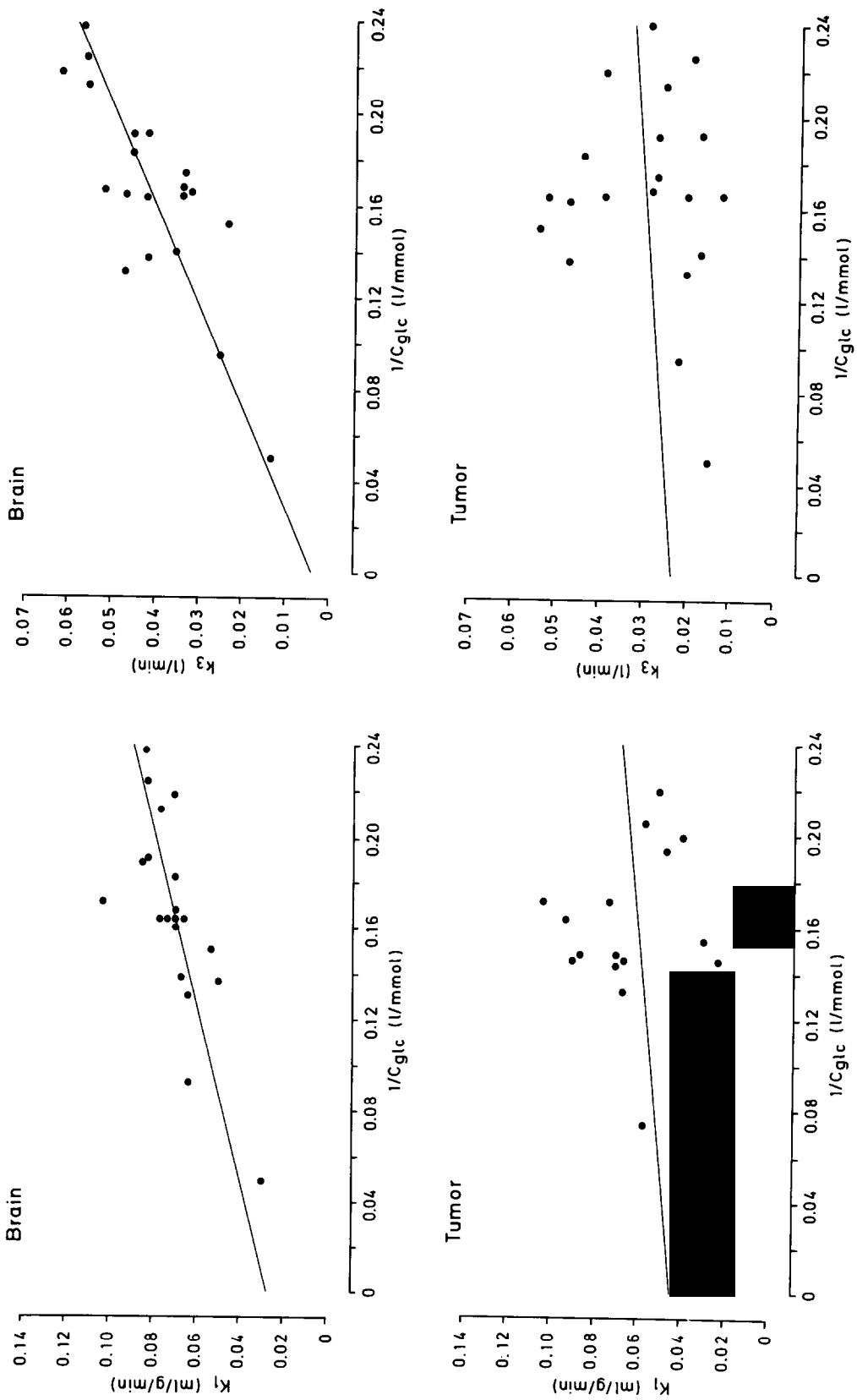

Fig. 6. Regression of transport and phosphorylation rate constants, K_1 (left) and k_3 (right), on the inverse of plasma glucose ($1/C_{glc}$). Highly significant relation due to competitive inhibition in contralateral brain tissue (top), but no relation in brain tumors (bottom).

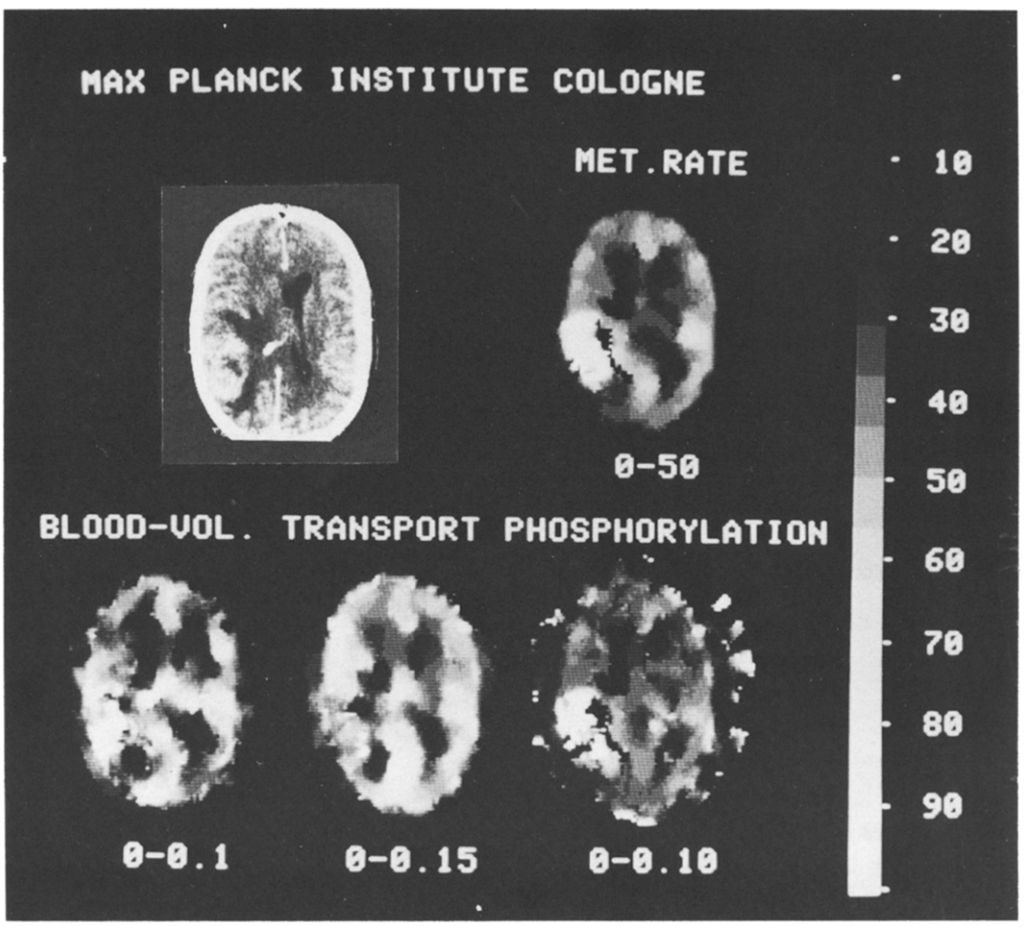

Fig. 2. X-Ray CT with i.v. contrast material (top row, left) and parametric FDG–PET images (glucose metabolic rate in μmol/100 g/min, *local blood volume in* ml/g, *transport rate constant* K_1 *in* ml/g/min, *and phosphorylation rate constant* k_3 *in* l/min) *of a right temporal glioblastoma (patient 15) with hypermetabolic, contrast enhancing rim around central necrosis. Good vascularization but normal or even slightly decreased FDG transport in hypermetabolic area. Value ranges are displayed below each image; the gray scale numbers indicate percentage values of individual range. Patient's left is on viewer's right.*

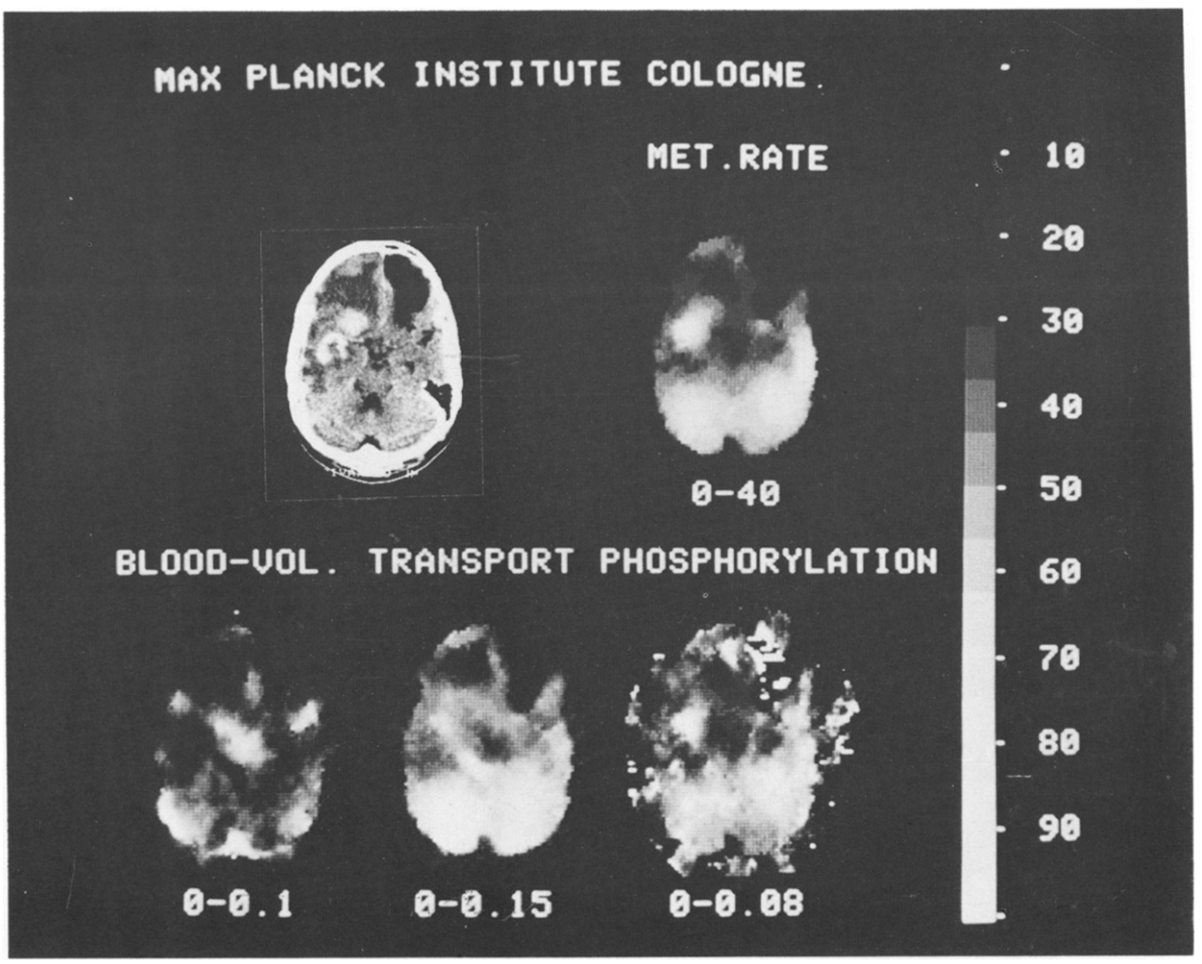

Fig. 3. X-Ray CT (with contrast material) and parametric FDG–PET images (same arrangement as in Fig. 2) of recurrent right fronto-temporal grade III glioma, 27 mm above canthomeatal plane. Note left frontal defect due to previous surgery, and right fronto-temporal, hypermetabolic, contrast enhancing tumor mass. FDG transport is largest in the cerebellum and only slightly increased in the tumor. The blood volume image shows mainly the major vessels (cavernous and transverse sinuses, confluens sinuum, anterior and middle cerebral arteries). The phosphorylation rate constant image is relatively noisy, with artifacts in low-counting rate areas (defect and outside of brain), but the area of high phosphorylation rate within the tumor can still be identified.

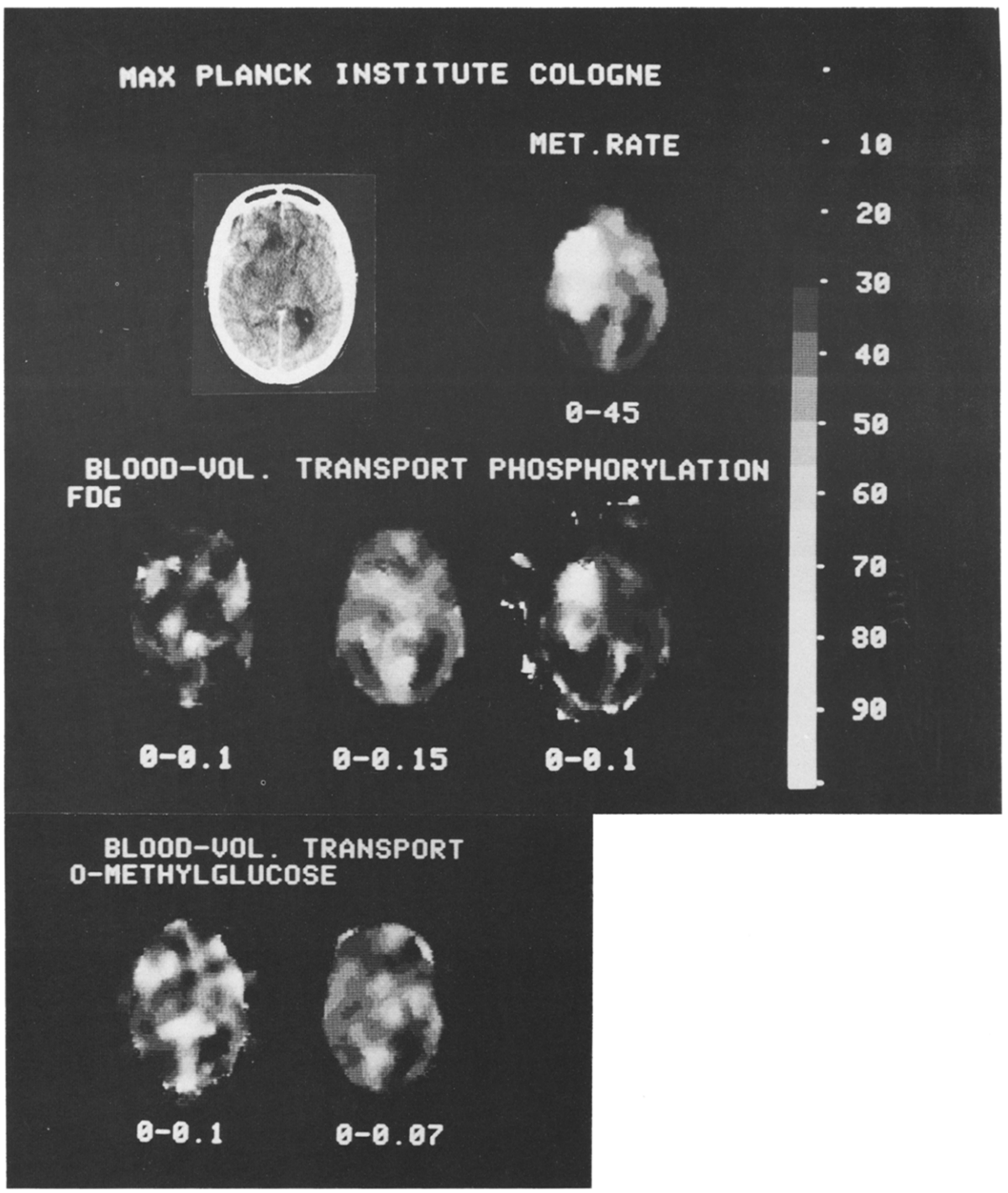

Fig. 4. X-Ray CT (with contrast material) and parametric FDG–PET images (same arrangement as in Fig. 2) of a right fronto-temporo-parietal grade III glioma (patient 5) at 54 mm above canthomeatal plane; in addition, at the bottom row, corresponding C-11-D-methylglucose parametric images of blood volume and transport rate constant are shown. The large, non-contrast enhancing, clinically highly malignant tumor exhibits high FDG phosphorylation, e.g. in its anterior part, but normal transport of both glucose analogs. Its middle part is poorly, the anterior and posterior parts are well, vascularized.

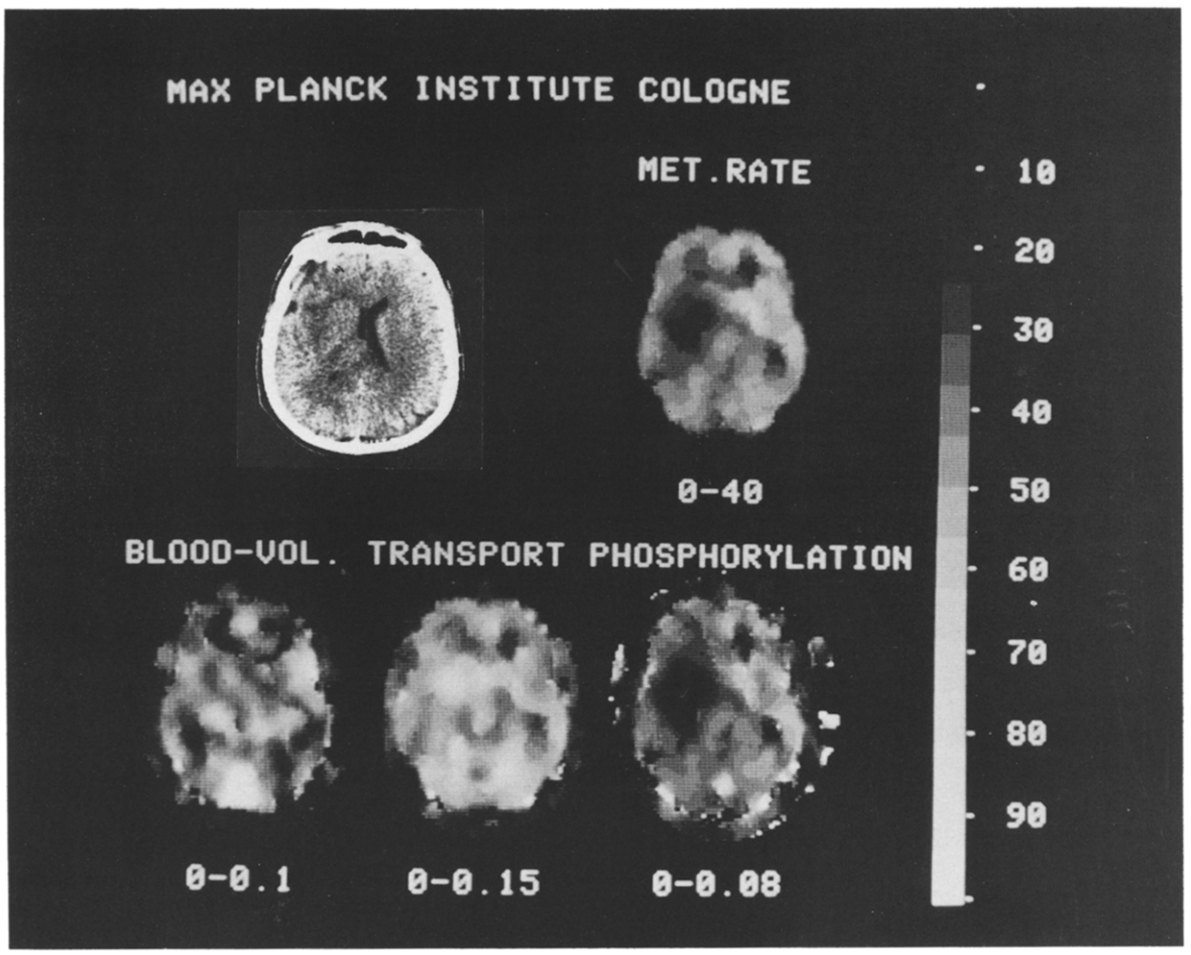

Fig. 5. X-Ray CT (with contrast material) and parametric FDG–PET images (same arrangement as in Fig. 2) of deep right temporal grade III glioma at 40 mm *above canthomeatal plane. The non-contrast enhancing tumor shows very low phosphorylation but normal FDG transport and vascularization.*

ual rate constants with histological grade was not significant. Nine tumors had very inhomogeneous metabolism. In two glioblastomas, a rim of increased metabolism was found around a central necrotic area (Fig. 2). On CT scans, this pattern corresponded with a contrast enhancing rim around a low-density central core in the two cases. In seven cases (three glioblastomas, four recurrent gliomas), areas of focally increased metabolism were seen at the periphery of the tumor. Only in three of these cases, was a corresponding area of contrast enhancement seen on CT scan (Fig. 3), while in the others the metabolically active area did not show distinct X-ray features.

In most cases, the hypermetabolic areas showed little or no increase of FDG transport (Figs. 2 and 3), indicating uncoupling of FDG transport and phosphorylation. Correspondingly there was no significant correlation between K_1 and k_3 (Pearson correlation coefficient $R = 0.15$) in tumors, in contrast to contralateral tissue where a moderate, albeit significant correlation ($R = 0.49$, $P = 0.028$) was observed. Uncoupling was most conspicuous in a large grade III glioma (patient 5, Fig. 4). There was a relatively homogeneous increase in FDG metabolism (mean 35.5 μmol/100 g/min in tumor vs. 16.3 in contralateral brain) but only a minor increase in FDG transport ($K_1 = 0.065$ vs. 0.054 ml/g/min). In this case, a [^{11}C]*O*-methylglucose (OMG) study was also performed (Fig. 4, bottom row), which confirmed normal hexose transport in the tumor [K_1 (OMG) = 0.027 ml/g/min in tumor vs. 0.026 in contralateral brain]. Another grade III glioma (anaplastic astrocytoma, patient 7, Fig. 5) also showed distinct uncoupling, but in this case, very low tumor metabolism (10.0 μmol/100 g/min vs. 17.7 in contralateral brain tissue) was in contrast with a slightly increased transport rate (0.090 vs. 0.070 ml/100 g/min).

Because FDG and unlabelled glucose compete at the carrier and hexokinase enzyme, an inverse relation between plasma glucose and rate constants K_1 and k_3 may be expected. Actually, a highly significant regression of K_1 ($F_{1,19} = 19.31$, $P = 0.0003$) and k_3 ($F_{1,19} = 38.26$, $P = 0.0001$) on the inverse of the plasma glucose level was observed in contralateral brain tissue (Fig. 6a, b). However, this relation was not preserved in tumor tissue (Fig. 6c, d). Neither the regression of mean tumor K_1 ($F_{1,19} = 0.893$, $P = 0.357$) nor of k_3 ($F_{1,19} = 0.263$, $P = 0.614$) on the inverse of plasma glucose concentration was significant.

A significant difference between the regression lines of tumor and brain k_3, respectively, on the inverse of plasma glucose was found using multivariate Hotelling–Lawley tracer statistics ($F_{1,18} = 5{,}361$, $P = 0.033$). Basically, the same results were obtained for mean K_1 and k_3 values in small circular regions of 10 mm diameter comprising the solid tumor core rather than the whole tumor, which in some cases included necrotic parts. There was no significant dependence of tumor core values on the inverse of plasma glucose.

Blood volume images were useful for estimating tumor vascularity relative to contralateral brain (Figs. 2–5). However, no close relation between histological grade or other clinical variables and tumor vascularity was detected.

DISCUSSION

The present report focusses on the uncoupling of FDG transport and metabolism in human gliomas. A close correspondence of glucose supply and metabolic needs has been demonstrated in normal brain by an experimental study [16]. Accordingly, a significant correlation between FDG transport and phosphorylation rate constants was found in contralateral brain, although the correlation coefficient was slightly smaller than observed previously in healthy subjects [11]. This may be due to variable metabolic depression of contralateral brain tissue in tumor patients. In contrast, no correlation between FDG transport and phosphorylation was observed in brain tumors. Both suppression of FDG phosphorylation (patient 7, Fig. 4) and large increases in phosphorylation (patient 14, Fig. 2) were observed in malignant gliomas, without much change of hexose transport. The interindividual variability of FDG transport and phosphorylation in brain tumors was so large that the normal inverse relation between competing plasma glucose and FDG rate constants was lost. This finding indicates that the activities of the corresponding enzymes vary much more in tumors than in normal brain tissue. It does, however, not imply a loss of competition between unlabelled plasma glucose and FDG within individual brain tumors.

Disruption of the blood–brain barrier could theoretically cause alterations of FDG transport. This possibility was however considered as unlikely by DiChiro *et al.* [17] and Hawkins *et al.* [12]. Preliminary data from this laboratory also suggest that there is no significant correlation between blood–brain barrier permeability to substances like [^{68}Ga]EDTA and alterations of FDG transport or phosphorylation [18]. The present *in vivo* data correspond well to changes of hexokinase activity observed *in vitro* in glioma cells [3, 19, 20] and in an experimental deoxyglucose study [21].

In a review of 100 cases and in previous papers, DiChiro [5] reported a correlation between histological tumor grade and glucose metabolism as measured with FDG–PET. Our data show a similar trend, which is best demonstrated by ratios of tumor

peak-to-contralateral brain metabolic rate (Fig. 1) because malignant tumors cause a suppression of glucose metabolism in remote gray matter [22]. Absence of a 'hot' area apparently does not exclude tumor malignancy, but its presence appears to be a strong indicator of malignancy and poor prognosis [5, 23].

We did not observe a significant effect of tumor location on metabolism, as suggested by Tyler *et al.* [24], but any firm statements concerning that issue are precluded by the small sample size. The same applies to possible effects of tumor radiation and chemotherapy, which could not be demonstrated.

The finding of uncoupling of tumor phosphorylation bears implications with regard to quantification of glucose metabolism by FDG studies. If the calculation of the metabolic rate is based on single scans only, as proposed by the adaptation of the original autoradiographic deoxyglucose method [25] to PET [26], fixed values for the rate constants must be assumed, which may lead to considerable errors if their normal relation is distorted—as is the case in tumors. This problem is overcome in the present approach by determination of the individual rate constants. However, there remains another problem. Differences between the affinities of glucose and FDG to the blood–brain carrier enzyme and the hexokinase are taken into account by the lumped constant [25]. Its value may change, if the relation between transport and phosphorylation changes. In particular, an increase of phosphorylation relative to transport, which was also observed in an experimental tumor study [21], causes an increase in the lumped constant [27]. It is tempting to try to use the fitted rate constants to correct for that shift, as proposed by Hawkins *et al.* [12]. But as shown by Wienhard *et al.* [28] different approaches for that correction [29, 30] may yield contradictory results. Furthermore, it has been reported that hexokinase isoenzymes, whose distribution may change in brain tumors, show different relations of their affinities to deoxyglucose and glucose [20]. Considering these uncertainties, no attempt was made to correct for the variability of the lumped constant. Therefore, in our view, the metabolic rate in tumors as determined by FDG–PET cannot be regarded as a strictly quantitative measure of glucose metabolism, but as a measure of the activity of the first step of the glycolytic pathway with respect to fluorodeoxyglucose. Despite these theoretical limitations, a good correlation between FDG uptake measured by PET, and glucose consumption as well as hexokinase activity measured in cell cultures derived from tumor specimens, has been shown by Kornblith *et al.* [19].

In some previous studies [12, 24] rate constants were fitted on the basis of regional curves usually comprising the whole tumor. In comparison with that approach, parametric images account for tumor heterogeneity and provide the best information on the extent and location of focal metabolic abnormalities that can be obtained under the constraints of the counting statistics and spatial resolution of PET. This is of particular clinical interest in recurrent gliomas, where small metabolically active areas were frequently found in the periphery of large necrotic or metabolically inactive areas. Moreover, fits on a pixel-by-pixel basis reduce the potential bias of nonlinear fits, which is caused by tissue heterogeneity [31]. The parametric images also provide information about the vascularization of a tumor, without requiring the application of another tracer as in previous studies [32]. Including blood volume in the fit of FDG uptake was feasible because it does not increase the variance of the rate constant estimates [12, 13].

The present study demonstrates that dynamic PET provides detailed information on the basic metabolic condition of brain tumors, which previously was available only by means of *in vitro* methods requiring tissue sampling. This appears to be of particular value considering the large biological heterogeneity even within histologically defined tumor classes. It is, therefore, conceivable that improved knowledge of the metabolic properties of each individual brain tumor may eventually lead to a more specific and individually optimized tumor therapy.

REFERENCES

1. Lust WD, Schwartz JP, Passonneau JV. Glycolytic metabolism in cultured cells of the nervous system. I. Glucose transport and metabolism in the C-6 glioma cell line. *Mol Cell Biochem* 1975, **8**, 169–176.
2. Keller K, Lange K, Noske W. D-Glucose transport of cultured cells of neural origin: the membrane as possible control point of glucose utilization. *J Neurochem* 1981, **36**, 1012–1017.
3. Lowry OH, Berger SJ, Carter JG *et al.* Diversity of metabolic patterns in human brain tumors: enzymes of energy metabolism and related metabolites and cofactors. *J Neurochem* 1983, **41**, 994–1010.
4. DiChiro G, DeLaPaz RL, Brooks RA *et al.* Glucose utilization of cerebral gliomas measured by [^{18}F]fluorodeoxyglucose and positron emission tomography. *Neurology* 1982, **32**, 1323–1329.

5. DiChiro G. Positron emission tomography using [^{18}F]fluorodeoxyglucose in brain tumors. A powerful diagnostic and prognostic tool. *Invest Radiol* 1986, **22**, 360–371.
6. Ido T, Wan CN, Fowler JS, Wolf AP. Fluorination with F_2, a convenient synthesis of 2-deoxy-2-fluoro-D-glucose. *J Org Chem* 1977, **42**, 2341–2342.
7. Ehrenkaufer RE, Potocki JF, Jewett DM. Simple synthesis of F-18-labeled 2-fluoro-2-deoxy-D-glucose: concise communication. *J Nucl Med* 1984, **25**, 333–337.
8. Eriksson L, Bohm C, Kesselberg M *et al.* A four ring positron camera system for emission tomography of the brain. *IEEE Trans Nucl Sci* 1982, **29**, 539–543.
9. Bergström M, Litton J, Eriksson L *et al.* Determination of object contour from projections for attenuation correction in cranial positron emission tomography. *J Comput Assist Tomogr* 1982, **6**, 365–372.
10. Bergström M, Eriksson L, Bohm C *et al.* Correction for scattered radiation in a ring detector positron camera by integral transformation of the projections. *J Comput Assist Tomogr* 1983, **7**, 42–50.
11. Heiss WD, Pawlik G, Herholz K *et al.* Regional kinetic constants and cerebral metabolic rate for glucose in normal human volunteers determined by dynamic positron emission tomography of [^{18}F]2-fluoro-2-deoxy-D-glucose. *J Cereb Blood Flow Metabol* 1984, **4**, 212–223.
12. Hawkins RA, Phelps ME, Huang SC. Effects of temporal sampling, glucose metabolic rates, and disruptions of the blood–brain barrier on the FDG model with and without a vascular compartment: studies in human brain tumors with PET. *J Cereb Blood Flow Metabol* 1986, **6**, 170–183.
13. Evans AC, Diksic M, Yamamoto YL *et al.* Effect of vascular activity in the determination of rate constants for the uptake of ^{18}F-labeled 2-fluoro-2-deoxy-D-glucose: error analysis and normal values in older subjects. *J Cereb Blood Flow Metabol* 1986, **6**, 724–738.
14. Patlak CS, Blasberg RG, Fenstermacher JD. Graphical evaluation of blood-to-brain transfer constants from multiple-time uptake data. *J Cereb Blood Flow Metabol* 1983, **3**, 1–7.
15. Alpert NM, Eriksson L, Chang J *et al.* Strategy for the measurement of regional cerebral blood flow using short-lived tracers and emission tomography. *J Cereb Blood Flow Metabol* 1984, **4**, 28–34.
16. Hawkins RA, Mans AM, Davis DW, Hibbard LS, Lu DM. Glucose availability to individual cerebral structures is correlated to glucose metabolism. *J Neurochem* 1983, **40**, 1013–1018.
17. DiChiro G, Brooks RA, Patronas NJ *et al.* Issues in the *in vivo* measurement of glucose metabolism of human central nervous system tumors. *Ann Neurol* 1984, **15** (Suppl), S138–S146.
18. Herholz K, Ziffling P, Staffen W *et al.* Correlative studies of glucose availability, glucose metabolism, BBB permeability, and extracellular volume in human brain tumors with PET. *J Cereb Blood Flow Metabol* 1987, **7** (Suppl. 1), S339.
19. Kornblith PL, Cummins CJ, Smith BH *et al.* Correlation of experimental and clinical studies of metabolism by PET scanning. *Prog Exp Tumor Res* 1984, **27**, 170–178.
20. Dominguez JE, Graham JF, Cummins CJ *et al.* Enzymes of glucose metabolism in cultured human gliomas: neoplasia is accompanied by altered hexokinase, phosphofructokinase, and glucose-6-phosphate dehydrogenase levels. *Metabol Brain Dis* 1987, **2**, 17–30.
21. Kato A, Diksic M, Yamamoto YL, Feindel W. Quantification of glucose utilization in an experimental brain tumor model by the deoxyglucose method. *J Cereb Blood Flow Metabol* 1985, **5**, 108–114.
22. DeLaPaz RL, Patronas NJ, Brooks RA *et al.* Positron emission tomographic study of suppression of gray-matter glucose utilization by brain tumors. *AJNR* 1983, **4**, 826–829.
23. Patronas NJ, DiChiro G, Kufta C *et al.* Prediction of survival in glioma patients by means of positron emission tomography. *J Neurosurg* 1985, **62**, 816–822.
24. Tyler JL, Diksic M, Villemure JG *et al.* Metabolic and hemodynamic evaluation of gliomas using positron emission tomography. *J Nucl Med* 1987, **28**, 1123–1133.
25. Sokoloff L, Reivich M, Kennedy C *et al.* The [^{14}C]deoxyglucose method for the measurement of local cerebral glucose utilization: theory, procedure, and normal values in the conscious and anesthetized albino rat. *J Neurochem* 1977, **28**, 897–916.
26. Reivich M, Kuhl D, Wolf A *et al.* The [^{18}F]fluorodeoxyglucose method for the measurement of local cerebral glucose utilization in man. *Circ Res* 1979, **44**, 127–137.
27. Pardridge WM. Brain metabolism: a perspective from the blood–brain barrier. *Physiol Rev* 1983, **63**, 1481–1535.
28. Wienhard K, Beil C, Heiss WD *et al.* Variations of the lumped constant in pathological conditions and during physiological stimulation. *J Cereb Blood Flow Metabol* 1987, **7** (Supp. 1), S481.
29. Gjedde A, Wienhard K, Heiss WD *et al.* Comparative regional analysis of 2-fluorodeoxyglucose and methylglucose uptake in brain of four stroke patients. With special reference to the regional estimation of the lumped constant. *J Cereb Blood Flow Metabol* 1985, **5**, 163–178.
30. Phelps ME, Huang SC, Mazziotta JC, Hawkins RA. Alternate approach for examining stability of the deoxyglucose model lumped constant. *J Cereb Flood Flow Metabol* 1983, **3** (Suppl. 1), S13–S14.

31. Herholz K, Patlak CS. The influence of tissue heterogeneity on results of fitting nonlinear model equations to regional tracer uptake curves: with an application to compartmental models used in positron emission tomography. *J Cereb Blood Flow Metabol* 1987, **7**, 214–229.
32. Lammertsma AA, Wise RJS, Cox TCS *et al.* Measurement of blood flow oxygen utilisation, oxygen extraction ratio, and fractional blood volume in human brain tumours and surrounding oedematous tissue. *Br J Radiol* 1985, **58**, 725–734.